Applied Physics B (2018) 124:117
https://doi.org/10.1007/s00340-018-6990-1

Applied Physics B
Lasers and Optics

Temperature and H_2O sensing in laminar premixed flames using mid-infrared heterodyne phase-sensitive dispersion spectroscopy

Liuhao Ma[1] · Zhen Wang[1] · Kin-Pang Cheong[1,2] · Hongbo Ning[1,2] · Wei Ren[1,2]

Received: 14 March 2018 / Accepted: 19 May 2018 / Published online: 29 May 2018

Abstract
We report the first demonstration of heterodyne phase-sensitive dispersion spectroscopy (HPSDS) for the simultaneous temperature and H_2O concentration measurements in combustion environments. Two continuous-wave distributed-feedback quantum cascade lasers (DFB-QCLs) at 5.27 and 10.53 μm were used to exploit the strong H_2O transitions (1897.52 and 949.53 cm^{-1}) at high temperatures. The injection current of each QCL was modulated at sub-GHz or GHz to generate the three-tone radiation and the dispersion signal was detected by the radio-frequency down-conversion heterodyning. The peak-to-peak ratio of the two H_2O dispersion spectra exhibits a monotonic relationship with temperature over the temperature range of 1000–3000 K, indicating the capability of performing two-line thermometry using laser dispersion spectroscopy. We measured the temperatures of CH_4/air flames at different equivalence ratios ($\Phi = 0.8$–1.2), yielding a good agreement with the corresponding thermocouple measurements. In addition, one-dimensional kinetic modeling coupled with a detailed chemical kinetic mechanism (GRI 3.0) was conducted to compare with the measured H_2O concentrations using HPSDS. Finally, we demonstrated HPSDS is immune to optical power fluctuations by measuring the dispersion spectra at varied incident laser powers.

1 Introduction

Laser-based optical diagnostics are receiving a continuous attention by the combustion community [1–5]. Among various optical diagnostics, laser absorption spectroscopy (LAS) is one of the most widely used methods due to its quantitative and non-intrusive measurement, high sensitivity and selectivity, fast time response, and relatively simple setup [6, 7]. Since its first demonstration in combustion measurement by Hanson et al. [8] in 1977, LAS has been rapidly developed and successfully applied in numerous combustion chemistry studies in shock tubes and laboratory flames. In addition to the fundamental combustion research, LAS-based sensors have been also used for monitoring the practical combustion and propulsion systems such as power plants, gas turbines, IC engines and scramjets. An excellent review of LAS in recent combustion measurements can be found elsewhere [9].

In LAS measurements, scanned-wavelength direct absorption (DA) and wavelength modulation spectroscopy (WMS) are two common techniques used for combustion diagnostics [9]. Due to the property of optical intensity measurement, it is essential to suppress or eliminate optical disturbances caused by beam steering, particle scattering, and broadband absorption in combustion. Additionally, when measuring optical intensity using a photodetector, LAS has intrinsic limitations such as the limited dynamic range (quantifying small changes in the total photo-detected laser intensity), the nonlinear response of the transmitted intensity to gas concentration (especially for strong absorption), and the direct impact of the intensity noise on the measured absorption signal.

Dispersion is a process accompanying gas absorption that affects the phase of electromagnetic radiation. It is known that dispersion is related to the frequency-dependent absorption coefficient via the Kramers–Kronig relation [10]. Hence, the spectroscopic information can also be inferred

This article is part of the topical collection "Mid-infrared and THz Laser Sources and Applications" guest edited by Wei Ren, Paolo De Natale and Gerard Wysocki.

✉ Wei Ren
renwei@mae.cuhk.edu.hk

[1] Department of Mechanical and Automation Engineering, The Chinese University of Hong Kong, New Territories, Hong Kong SAR, China

[2] Shenzhen Research Institute, The Chinese University of Hong Kong, New Territories, Hong Kong SAR, China

from the dispersion spectrum associated with the refractive index. A series of experiments have recently demonstrated the capability of using dispersion spectroscopy for trace gas sensing [11–16] with the merits of immunity to laser power fluctuations and calibration-free operations. The direct dispersion measurement can be achieved using chirped laser dispersion spectroscopy (CLaDs) [11] and heterodyne phase-sensitive dispersion spectroscopy (HPSDS) [12]. CLaDs adopts a frequency-chirped laser to transform optical phase variation into frequency shift which can be used for the recovery of dispersion spectra [11]. In comparison, HPSDS has the advantages of simpler optical configurations and data acquisition processes by directly modulating the optical intensity or injection current of the semiconductor lasers to generate spectral sidebands [12]. Note that frequency modulation spectroscopy (FMS) enables the access of optical absorption and dispersion, but the dispersion information is rarely used for sensing applications. The recuperative dispersion spectra may also be partially distorted using FMS [12]. Moreover, FMS is a derivative method of LAS employing high-frequency modulation and has the same limitation of absorption-based techniques due to the actual light amplitude detection. Frequency comb spectroscopy (FCS) is another technique that enables measuring both molecular absorption and dispersion [17, 18], but the FCS detection using dispersion-based sensing method is technically complex and challenging [18].

The first demonstration of HPSDS for gas sensing was performed by Martín-Mateos and Acedo [12]. In that work, CH_4 was measured using a vertical-cavity surface-emitting laser (VCSEL) near 1.65 μm and an analytical model was proposed to describe the entire dispersion process. This method was later extended to the mid-infrared gas detection of CO by the same group using a quantum cascade laser (QCL) near 4.59 μm [15]. However, very few studies have been reported so far to use laser dispersion spectroscopy for combustion measurements. Considering the intrinsic advantages of the immunity to laser intensity fluctuations, mitigation of photodetector nonlinearity, and high dynamic range due to the phase detection [19], laser dispersion spectroscopy is possibly a good candidate for combustion diagnostics. Recently, we have measured the dispersion spectra of several CO_2 transitions (2390.52, 2391.10, 2391.65 and 2392.18 cm^{-1} in the v_3 fundamental band) in laminar flames under sooting and non-sooting conditions using HPSDS [20]. The CO_2 mole fractions can be successfully inferred from the measured dispersion spectra with the known flame temperatures determined by thermocouples.

In this work, we report the simultaneous temperature and H_2O sensing in flames using HPSDS for the first time. Two continuous-wave distributed-feedback (DFB) QCLs were employed to probe two strong H_2O lines at the wavelengths near 5.27 μm and 10.53 μm, respectively. These two H_2O lines have a difference of 3945.5 cm^{-1} in the lower state energy E'' to ensure sensitive temperature measurements. The corresponding dispersion spectra of H_2O were measured in premixed CH_4/air flames above a McKenna burner. The flame temperature was inferred using two-line thermometry based on the measured two dispersion spectra. Additionally, the thermocouple measurements and CHEMKIN simulations were performed to compare with the laser dispersion measurements.

2 Spectroscopic fundamentals

Laser dispersion spectroscopy measures the phase information associated with the refractive index variation of gas medium that is inherent to a molecular transition. When the laser wavelength is tuned close to the transition (i.e., rotational, vibrational and electronic), absorption and dispersion of the incident laser radiation occur simultaneously. The refractive index is related to the frequency-dependent absorption coefficient via the Kramers–Kronig equation [10]:

$$n(\omega) = 1 + \frac{c}{\pi}\int_0^{+\infty} \frac{\alpha(\omega')}{\omega'^2 - \omega^2} \mathrm{d}\omega', \tag{1}$$

where $n(\omega)$ and $\alpha(\omega)$ are the refractive index and absorption coefficient at the optical angular frequency ω, respectively; and c is the speed of light in vacuum. Hence, the dispersion measurement can be performed instead of laser intensity measurement to retrieve the same spectroscopic information as that using LAS.

For mid-infrared laser sources such as QCLs, a fast modulation of the laser injection current at an angular frequency Ω generates a three-tone radiation. As schematically shown in Fig. 1, the modulated QCL radiation contains one central tone (E_1) at ω_0 and two sidebands (E_2, E_3) at $\omega_0 \pm \Omega$, respectively. Meanwhile, an additional intensity modulation (IM) of the QCL accompanies the frequency modulation (FM) [21–23]. Hence, the three-tone radiation can be expressed as [22]:

$$E_1 = I\cos(\omega_0 t), \tag{2}$$

$$E_2 = \frac{a}{4} I\left\{\cos[(\omega_0 + \Omega)t] + \frac{2b}{a}\cos[(\omega_0 + \Omega)t - \phi]\right\}, \tag{3}$$

$$E_3 = \frac{a}{4} I\left\{\cos[(\omega_0 - \Omega)t] - \frac{2b}{a}\cos[(\omega_0 - \Omega)t + \phi]\right\}, \tag{4}$$

where I is the laser intensity, a is the IM index (amplitude of IM divided by the total intensity), b is the FM index (amplitude of FM divided by the modulation frequency), and ϕ is the phase shift between FM and IM.

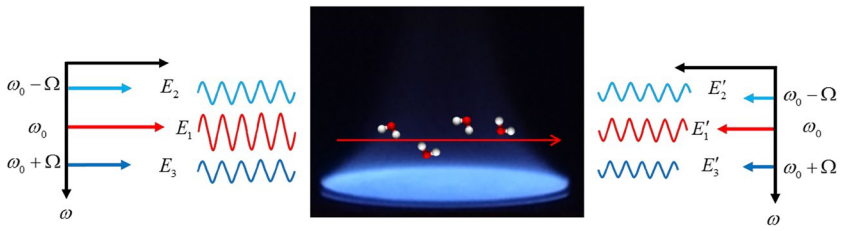

Fig. 1 Schematic of the three-tone beam traveling through a laminar premixed flame

After traveling through the gas medium with a path length of L, the three tones of the QCL interact with the target molecule (i.e., H_2O in this work) and experience different phase shifts induced by dispersion and intensity attenuation due to gas absorption near the target absorption line. The transmitted three-tone laser radiation (E_1', E_2', and E_3') can be expressed as:

$$E_1' = e^{-\frac{\alpha(\omega_0)L}{2}} I\cos(\omega_0 t - \psi_1), \tag{5}$$

$$E_2' = e^{-\frac{\alpha(\omega_0+\Omega)L}{2}} \frac{a}{4} I\left\{\cos[(\omega_0+\Omega)t - \psi_2] + \frac{2b}{a}\cos[(\omega_0+\Omega)t - \phi - \psi_2]\right\}, \tag{6}$$

$$E_3' = e^{-\frac{\alpha(\omega_0-\Omega)L}{2}} \frac{a}{4} I\left\{\cos[(\omega_0-\Omega)t - \psi_3] - \frac{2b}{a}\cos[(\omega_0-\Omega)t + \phi - \psi_3]\right\}, \tag{7}$$

where ψ_1, ψ_2 and ψ_3 are the phase shifts of the three tones induced by dispersion, and $\alpha(\omega_0)$, $\alpha(\omega_0+\Omega)$ and $\alpha(\omega_0-\Omega)$ are the absorption coefficients. The transmitted laser beam impinges on a square-law photodetector and generates a radio frequency (RF) beat note signal that can be expressed as:

$$I = (E_1' + E_2' + E_3')^2. \tag{8}$$

Hence, the dispersion information is encoded in the phase of the beat note component at the same frequency (Ω) as the laser modulation frequency. The detected beat note signal is then downshifted by a mixer to the frequency range of the lock-in amplifier to obtain the dispersion information. Once the dispersion spectra of two absorption lines with different lower state energies are measured, temperature can be retrieved using the standard two-line thermometry method [24].

3 Method

3.1 Wavelength selection

As dispersion is relevant to absorption by the Kramers–Kronig relation, we used the similar line selection rules as that for LAS by evaluating the line strength, spectral isolation, and temperature sensitivity. The strong H_2O absorption bands in the mid-infrared domain of 5–12 μm can be accessed readily by the commercial QCLs. In this work, we probed two H_2O lines at 949.53 cm^{-1} (10.53 μm) and 1897.52 cm^{-1} (5.27 μm), respectively, using two DFB-QCLs. Table 1 summarizes the spectroscopic parameters of the selected H_2O lines taken from the HITEMP 2010 database [25].

Figure 2a shows the simulated absorption coefficients of the selected H_2O lines at a typical flame condition of 1850 K, 1 atm, 18% H_2O, 8.5% CO_2, and 0.5% CO. Note that another H_2O line centered at 1897.37 cm^{-1} is adjacent to one of our target lines. The simulation results indicate that the spectral interferences from CO_2 and CO are negligible for H_2O measurements in these two wavelength regions. In addition, due to the large E'' (> 2000 cm^{-1}) for both H_2O lines, the ambient cold water vapor has little influence on the measurement even for a meter-long open path, making the diagnostic more flexible in actual flame measurements. The LAS-based temperature sensitivity of the line pair selected in this work is plotted in Fig. 2b along with the comparison with the previous study using the line pair of H_2O at 2.5 μm [24]. It is evident that the current line pair has a better sensitivity over the temperature range of 1000–3000 K.

Table 1 Spectroscopic parameters of the selected H_2O lines (HITEMP 2010 [25])

Line	Frequency (cm^{-1})	Wavelength (nm)	S@296K (cm^{-2}/atm)	E'' (cm^{-1})
1	949.53	10531.53	1.405×10^{-10}	5987.8
2	1897.52	5270.04	2.648×10^{-3}	2042.3

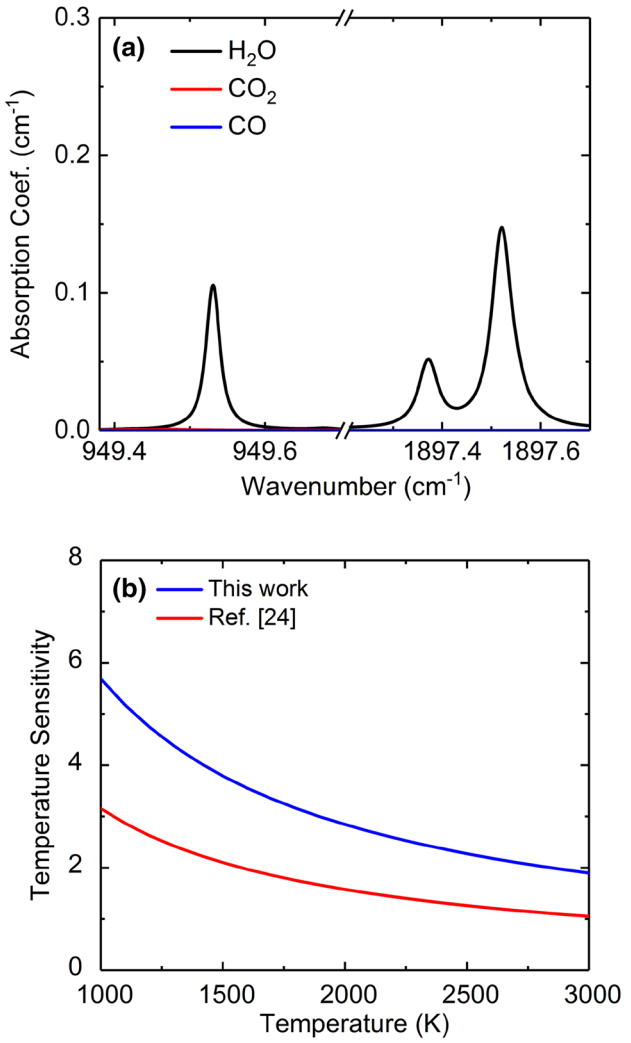

Fig. 2 **a** Spectral simulation of the major species (18% H_2O, 8.5% CO_2, and 0.5% CO) in laminar premixed flames at 1850 K and 1 atm at the wavelengths of 5.27 and 10.53 μm. **b** Comparison of the temperature sensitivity of the line pair selected in this study with that at 2.5 μm [24]

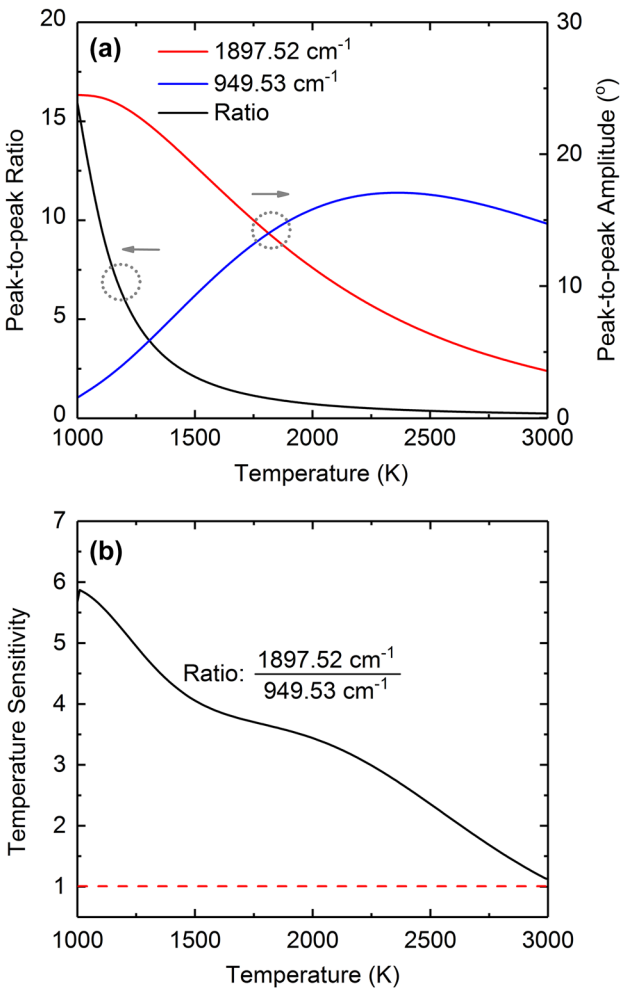

Fig. 3 **a** Simulated peak-to-peak amplitudes of H_2O dispersion signals at 1897.52 and 949.53 cm^{-1} and the corresponding ratio as a function of temperature. Simulation is performed at conditions: $P = 1$ atm, $T = 1000 - 3000$ K, $X_{H2O} = 18\%$, and $L = 6$ cm. **b** Temperature sensitivity of the dispersion-based H_2O two-line thermometry

The peak-to-peak amplitude of the dispersion signal is normally used in gas sensing applications to infer gas concentration. Here, we further explore the relationship between temperature and the ratio of the peak-to-peak amplitudes of the selected two H_2O lines. Figure 3a presents the simulated peak-to-peak amplitudes of the two H_2O lines and the corresponding ratio over the temperature range of 1000–3000 K. The peak-to-peak ratio (R) changes monotonically with temperature over the entire temperature range. Hence, the two-line thermometry can also be adopted using laser dispersion spectroscopy for temperature sensing. For the dispersion-based two-line thermometry, we define the measurement sensitivity as the derivative of the peak-to-peak ratio with respect to temperature, or $|(dR/R)/(dT/T)|$, which indicates the unit change in the normalized ratio of peak-to-peak amplitude for a unit change in the normalized temperature. Figure 3b plots the temperature sensitivity of the selected H_2O line pair over the temperature range of 1000–3000 K. Hence, the current dispersion-based two-line thermometry can be used for sensitive temperature measurements (with sensitivity > 1) up to 3000 K.

3.2 Experimental setup

All the experiments were performed in laminar premixed methane–air flames (McKenna burner) stabilized above a sintered stainless-steel porous disk with a diameter of 60 mm. The flame was shielded by nitrogen co-flows coming from the sintered bronze shroud ring to eliminate the ambient interference. Further details of the gas supply and flame description are provided in our previous studies [24, 26].

Two DFB-QCLs were tuned to the target H_2O transitions by controlling the laser temperatures and injection currents using the low-noise laser drivers (ILX Lightwave, LDC-3736). Figure 4 depicts the wavelength tuning performance of the QCLs using a spectral analyzer. The two selected H_2O lines can be covered by scanning the injection current of the QCLs at a fixed temperature of 37 °C. Note that a relatively high injection current (~ 1 A) is required to drive the QCL at 10.53 µm.

Figure 5 illustrates the schematic of the optical setup. The QCL current was scanned by a ramp signal and sinusoidally modulated by an RF signal generator (RF-SG_1) at a relatively high frequency. The dispersion measurements for the two H_2O lines at 949.53 and 1897.52 cm^{-1} were performed at the optimal modulation frequencies of 400 MHz and 1 GHz, respectively, to maximize the peak-to-peak amplitude. Note that the optimal modulation frequency is relevant to the full width at half maximum (FWHM) of the target line [12], and is found to be 0.64–0.67 times the FWHM of the two H_2O lines detected by the current QCLs. The generated three-tone laser beams passed through the flame and were then collected by a concave mirror onto a high-speed HgCdTe photodetector (VIGO System S.A., PVI-4TE-10.6, 1 GHz bandwidth) to produce the heterodyne beat note signals (PD_1 and PD_2 shown in Fig. 5a). The narrow-bandpass filters were used to reduce the thermal backgrounds. The detected beat note signal was mixed with another RF sinusoidal signal (100 kHz different from the QCL modulation frequency) generated by RF-SG_2 shown in Fig. 5b. Thus, the beat note was downshifted to the frequency range that can be accessed by a lock-in amplifier. Note that the lock-in amplifier used the reference signal (100 kHz) generated by the difference of the two RF generators. The synchronization between RF-SG1 and RF-SG2 was achieved by using the 10 MHz timebase interface of the RF generators.

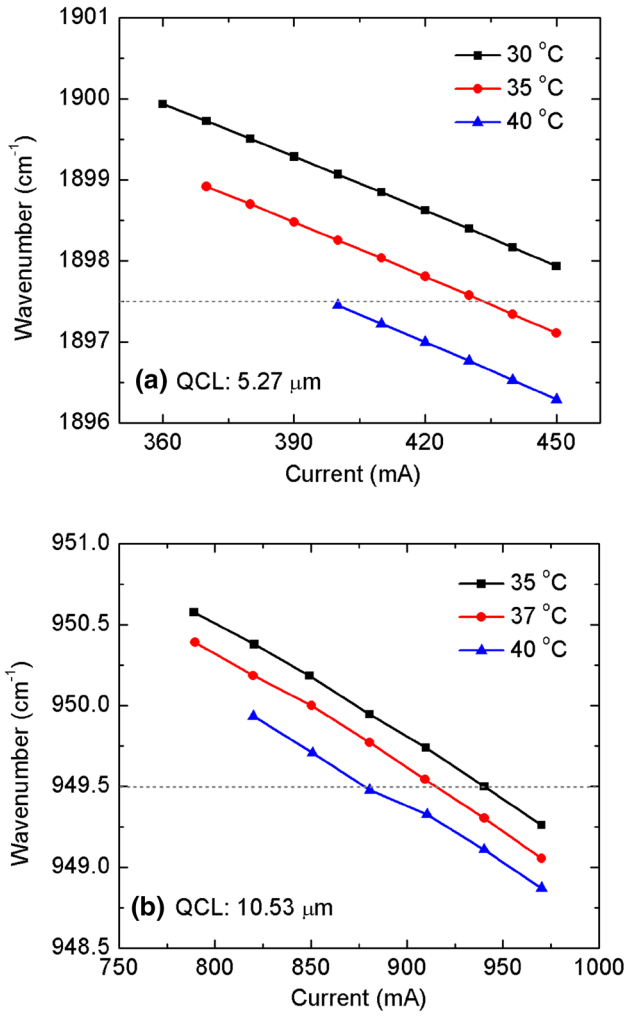

Fig. 4 Wavelength tuning characteristics of the two DFB-QCLs used in this study

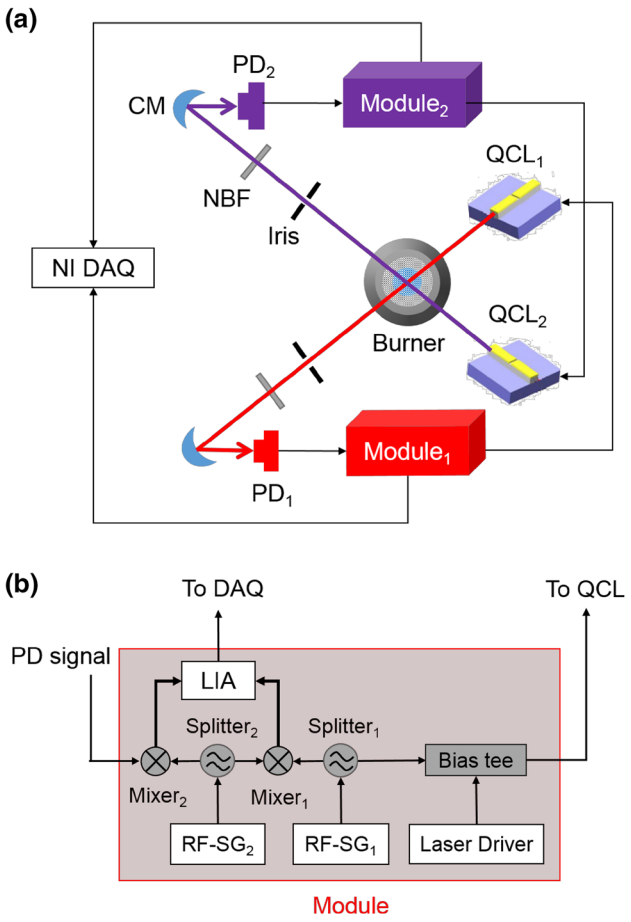

Fig. 5 **a** Schematic of the HPSDS system for flame measurements. QCL_1, quantum cascade laser at 10.53 µm; QCL_2, quantum cascade laser at 5.27 µm; CM, concave mirror; NBF, narrow-bandpass filter; PD, high-speed photodetector. **b** Schematic of the module used for QCL modulation and beat note detection. RF-SG RF signal generator; LIA lock-in amplifier; DAQ data acquisition card

4 Results and discussion

To validate the temperature measurement using dispersion spectroscopy, we also measured the flame temperature using a Pt/30%/Rh-Pt/6%/Rh thermocouple (Omega, Type B) and performed 1-D flame simulations using CHEMKIN-Pro software package [27]. The "Premixed Laminar Burner-stabilized Flame" model coupled with GRI 3.0 mechanism (53 species and 325 reactions) [28] was used for CH_4/air flame simulations.

All the HPSDS measurements were performed at 5 mm above the burner surface to ensure relatively uniform temperature and species concentration distributions. Figure 6 shows the representative dispersion spectra of the two selected H_2O lines in a laminar premixed CH_4/air flame at the stoichiometric condition. Note that the experimental data were obtained in a single measurement without any averaging operations. Temperature and H_2O mole fraction can be obtained by fitting the measured dispersion spectra using the spectroscopic model described in Sect. 2. Note that the characterized QCL parameters (IM index, FM index and the phase shift between FM and IM) and molecular spectroscopic parameters (line-strength, lower state energy, and broadening coefficient) were used as the input parameters for spectroscopic simulations.

Figure 7 presents the measured temperatures and H_2O mole fractions at different equivalence ratios ($\Phi = 0.8$–1.2). We compare the HPSDS-determined temperatures with the thermocouple measurements and CHEMKIN simulations. In general, the HPSDS measurements are in good agreement with the thermocouple results within 2% (mostly within 1.5% except for the case at $\Phi = 1.1$), and 3% different from the CHEMKIN simulations. The uncertainty of thermocouple measurement is estimated to be ~5.5% by taking into account the radiation correction and reading errors, which is detailed in our previous work [24]. The overall uncertainty of the HPSDS thermometry is estimated to be ~5.6% considering the spectral peak-to-peak fitting error (1%) and line-strength uncertainty (5%). In addition, the measured H_2O mole fractions at different equivalence ratios are compared with the CHEMKIN simulations shown in Fig. 7b. The measured H_2O mole fractions agree well with the CHEMKIN simulations, mostly within a relative difference of 0.5%. The maximum relative difference is ~1.1% at the equivalence ratio $\Phi = 1.2$. The major uncertainties of H_2O concentration measurements come from the line-strength and spectral fitting error, contributing to an overall uncertainty of ~5.6%.

We also performed several additional HPSDS measurements of H_2O to validate the intrinsic immunity to laser intensity fluctuations by varying the incident laser power. Figure 8 illustrates the peak-to-peak amplitudes of the two H_2O dispersion spectra measured at the stoichiometric

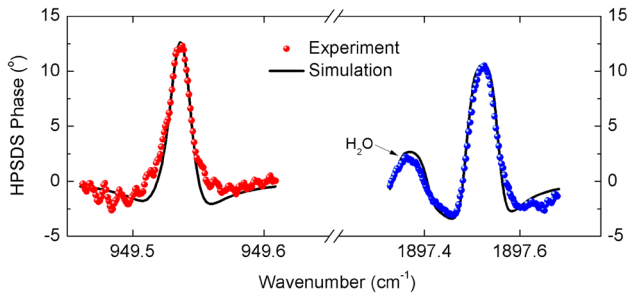

Fig. 6 Comparison of the measured HPSDS phase signals (symbol) and model fittings (solid line) of the two H_2O lines at 949.53 and 1897.52 cm^{-1}

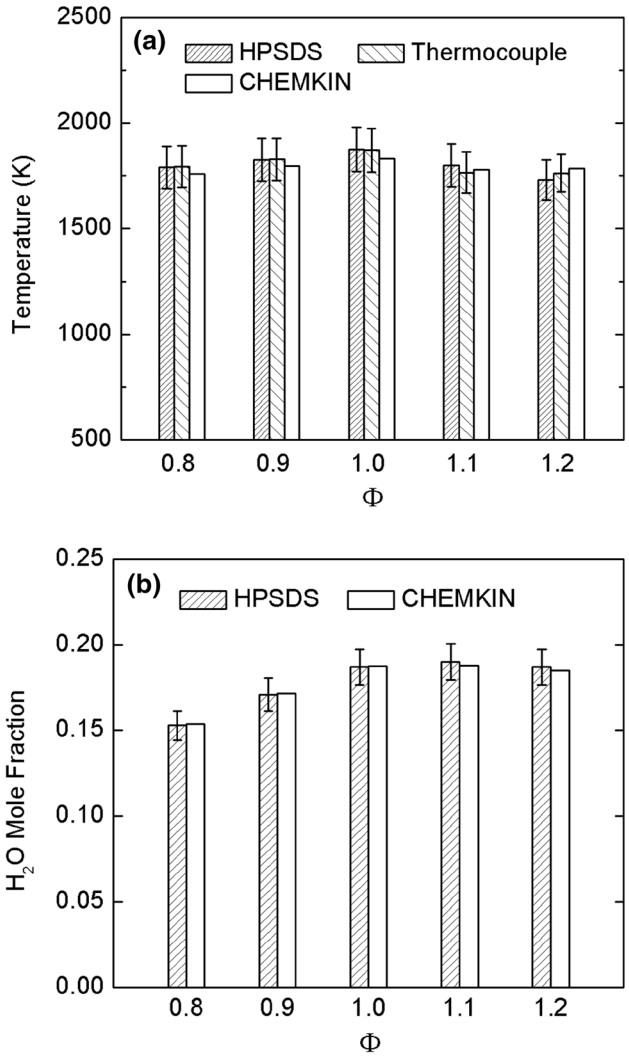

Fig. 7 Comparison of the measured and calculated **a** temperatures and **b** H_2O mole fractions in laminar premixed CH_4/air flames ($\Phi = 0.8$–1.2). The simulation is performed using GRI 3.0 mechanism [28] in CHEMKIN-Pro software

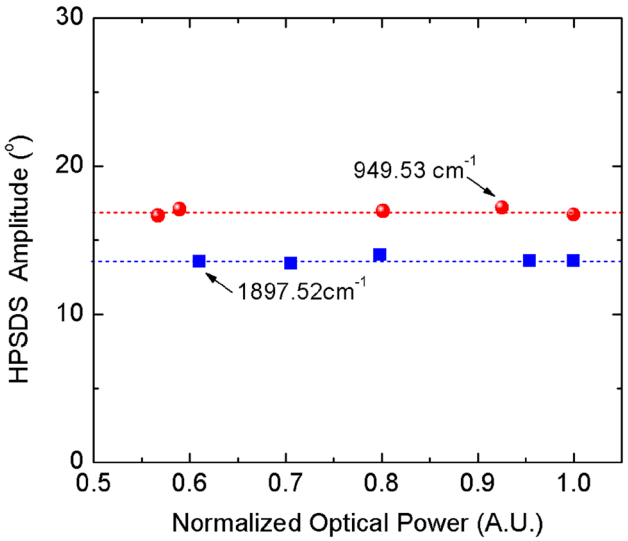

Fig. 8 Measured HPSDS amplitudes of H_2O at varied laser powers. The CH_4/air flame is at the stoichiometric condition

condition of the CH_4/air flame for different incident laser powers. The HPSDS peak-to-peak amplitude remains almost unchanged (standard deviation of 0.20° for 1897.52 and 0.21° for 949.53 cm^{-1}) with the laser power varied by 40%.

5 Conclusions

We reported the first simultaneous measurement of temperature and H_2O concentration in combustion environment using mid-infrared HPSDS. The dispersion measurements were performed by employing two direct injection-current-modulated QCLs at the modulation frequency of sub-GHz to GHz and detecting the heterodyne phase signals. The QCLs exploited two strong H_2O lines near 5.27 and 10.53 μm to achieve sensitive species and temperature measurements. We demonstrated the method of inferring the flame temperature using two-line thermometry based on the measured dispersion spectra of two H_2O lines with a large difference in the lower state energy. The HPSDS-determined H_2O mole fractions are in good agreement with the CHEMKIN model simulations. Future work will involve the application of this method for multi-species measurements in combustion systems and characterizations of non-uniform reacting flows. In particular, we expect the laser dispersion spectroscopy can be used for non-uniform combustion diagnostics by adopting the multi-line profile-fitting or tomography method [29, 30], with extra advantages of the immunity to laser power fluctuations in harsh environments.

Acknowledgements This research is supported by National Natural Science Foundation of China (NSFC) (51776179) and Research Grants Council of the Hong Kong Special Administrative Region, China (14234116). The authors gratefully acknowledge the National Supercomputing Center (Shenzhen) for providing CHEMKIN-Pro (15131) software and computational facilities.

References

1. C.A. Taatjes, N. Hansen, A. McIlroy, J.A. Miller, J.P. Senosiain, S.J. Klippenstein, F. Qi, L. Sheng, Y. Zhang, T.A. Cool, Science **308**(5730), 1887–1889 (2005)
2. C. Schulz, V. Sick, Prog. Energy Combust. Sci. **31**, 75–121 (2005)
3. R.K. Hanson, D.F. Davidson, Prog. Energy Combust. Sci. **44**, 103–114 (2014)
4. H. Michelsen, C. Schulz, G. Smallwood, S. Will, Prog. Energy Combust. Sci. **51**, 2–48 (2015)
5. W. Cai, C.F. Kaminski, Prog. Energy Combust. Sci. **59**, 1–31 (2017)
6. R.K. Hanson, Proc. Combust. Inst. **33**, 1–40 (2011)
7. R.K. Hanson, R.M. Spearrin, C.S. Goldenstein, *Spectroscopy and optical diagnostics for gases* (Springer, Switzerland, 2016)
8. R.K. Hanson, P.A. Kuntz, C.H. Kruger, Appl. Opt. **16**, 2045–2048 (1977)
9. C.S. Goldenstein, R.M. Spearrin, J.B. Jeffries, R.K. Hanson, Prog. Energy Combust. Sci. **60**, 132–176 (2017)
10. J.S. Toll, Phys. Review **104**, 1760 (1956)
11. G. Wysocki, D. Weidmann, Opt. Express **18**, 26123–26140 (2010)
12. P. Martín-Mateos, P. Acedo, Opt. Express **22**, 15143–15153 (2014)
13. M. Nikodem, G. Plant, D. Sonnenfroh, G. Wysocki, Appl. Phys. B **119**, 3–9 (2015)
14. W. Ding, L. Sun, L. Yi, X. Ming, Appl. Opt. **55**, 8698–8704 (2016)
15. P. Martín-Mateos, J. Hayden, P. Acedo, B. Lendl, Analyt. Chemistry **89**, 5916–5922 (2017)
16. S. Paul, P. Martín-Mateos, N. Heermeier, F. Küppers, P. Acedo, ACS Photonics **4**, 2664–2668 (2017)
17. C.A. Alrahman, A. Khodabakhsh, F.M. Schmidt, Z. Qu, A. Foltynowicz, Opt. Express **22**, 13889–13895 (2014)
18. P. Martín-Mateos, B. Jerez, P. Acedo, Opt. Express **23**, 21149–21158 (2015)
19. M. Nikodem, G. Wysocki, Opt. Lett. **38**, 3834–3837 (2013)
20. L. Ma, Z. Wang, K.-P. Cheong, H. Ning, W. Ren, Accepted for oral presentation in the 37th International Symposium on Combustion, Dublin, Ireland
21. H. Olesen, G. Jacobsen., IEEE J. Quantum Electron. **18**, 2069–2080 (1982)
22. A. Hangauer, G. Spinner, M. Nikodem, G. Wysocki, Appl. Phys. Lett. **103**, 191107 (2013)
23. A. Hangauer, G. Spinner, M. Nikodem, G. Wysocki, Opt. Express **22**, 23439–23455 (2014)
24. L. Ma, H. Ning, J. Wu, W. Ren, Combust. Sci. Technol. **190**, 392–407 (2018)
25. L.S. Rothman, I.E. Gordon, R.J. Barber, H. Dothe, R.R. Gamache, A. Goldman, V.I. Perevalov, S.A. Tashkun, J. Tennyson, J. Quant. Spectrosc. Radiat. Transf. **111**, 2139–2150 (2010)
26. L.H. Ma, L.Y. Lau, W. Ren, Appl. Phys. B **123**, 83 (2017)
27. Reaction Design (2013) *CHEMKIN-PRO 15131. Reaction design*, San Diego, CA
28. G.P. Smith, D.M. Golden, M. Frenklach, N.W. Moriarty, B. Eiteneer, M. Goldenberg, C.T. Bowman, R.K. Hanson, S. Song, W.C. Gardiner Jr., "GRI-Mech 3.0," URL: http://www.me.berkeley.edu/gri_mech/. Accessed 1 Feb 2018
29. S.T. Sanders, J. Wang, J.B. Jeffries, R.K. Hanson, Appl. Opt. **40**, 4404–4415 (2001)
30. L. Ma, W. Cai, A.W. Caswell, T. Kraetschmer, S.T. Sanders, S. Roy, J.R. Gord, Opt. Express **17**, 8602–8613 (2009)